Novel mechanisms of type IV pilus regulation in *Acinetobacter baylyi*

Courtney K. Ellison[1,2*], Triana N. Dalia[3], Catherine A. Klancher[3], Joshua W. Shaevitz[1*], Zemer Gitai[2*], and Ankur B. Dalia[3*]

1. Lewis-Sigler Institute for Integrative Genomics, Princeton University, Princeton, NJ
2. Department of Molecular Biology, Princeton University, Princeton, NJ
3. Department of Biology, Indiana University, Bloomington, IN

*Correspondence to: c.ellison@princeton.edu, shaevitz@princeton.edu, zgitai@princeton.edu, ankdalia@indiana.edu

Abstract

Bacteria employ extracellular appendages called type IV pili (T4P) to interact with their environment. T4P are essential for diverse microbial behaviors including DNA uptake, surface sensing, virulence, protein secretion, and twitching motility (*1*). While T4P have been studied extensively, our understanding of these nanomachines largely comes from work on a few model species. Here, we develop *Acinetobacter baylyi* as a new model organism to study T4P and uncover several unreported mechanisms of T4P regulation. First, using recently-developed T4P-labeling methods (*2*, *3*), we demonstrate that *A. baylyi* T4P are synthesized on one side of the cell body along the long axis of the cell, and we uncover that this pattern is dependent on components of a conserved chemosensory pathway. Second, we overturn the current dogma that T4P extension occurs through the action of a single, highly conserved ATP-hydrolyzing motor (ATPase) called PilB by showing that T4P synthesis in *A. baylyi* is dependent on two partially redundant and phylogenetically distinct motors, PilB and PilB2. Third, we uncover a small protein inhibitor of T4P synthesis that specifically inhibits PilB but not PilB2 activity. Together, these results demonstrate novel mechanisms of T4P regulation, which have broad implications for the unexplored diversity of T4P biology in microbial species.

Results and Discussion

T4P are thin, proteinaceous appendages that are broadly distributed throughout Bacteria and Archaea (*4*). T4P are composed primarily of major pilin protein subunits that are polymerized or depolymerized through the activity of ATPases to mediate fiber extension and retraction, respectively (*5*). T4P are subdivided into subcategories (generally T4aP, T4bP, and T4cP) based on protein homology and pilus function, with T4aP being the best-characterized. In the T4aP systems found in Gram-negative organisms, polymerization and depolymerization of pilins occurs through interactions of the extension ATPase PilB or retraction ATPase PilT with the integral inner membrane platform protein PilC (Supplemental figure 1a). The growing fiber spans an alignment complex from the inner membrane through the periplasm composed of PilNOP to exit through the PilQ outer membrane secretin pore. Dynamic cycles of T4P extension and retraction are critical for the diverse processes that these structures mediate including twitching motility (*6*), surface sensing (*2*, *7*), virulence (*8*, *9*), and DNA uptake (*10*, *11*).

Acinetobacter species like *A. baumannii* and *A. nosocomialis* have recently become an urgent medical threat due to their prevalence in hospital-acquired infections and their capacity to acquire antibiotic resistance genes, a process that is achieved in part by T4aP-mediated DNA uptake (*12*, *13*). *Acinetobacter baylyi* is the most naturally transformable species reported to date (*14*), with up to 50% of cells undergoing natural transformation in ideal settings. To study *A. baylyi* T4P, we applied a recently-developed labeling method (*2*, *3*) by targeting the major pilin, ComP, for cysteine substitution and subsequent labeling with thiol-reactive maleimide dyes. Maleimide-labeling of the functional *comP*^{T129C} strain (Supplemental figure 1b) revealed an unusual pattern of pilus synthesis, with T4P appearing only on one side of the cell body in a line along the long axis of the cell (Figure 1a). Deletion of the retraction ATPase, PilT, resulted in hyperpiliated cells exhibiting the same localization of T4P along the long axis of the cell. Cells with T4P facing the microscope objective show T4P localize linearly along the side of the cell where they are synthesized (Figure 1a). T4P localization has previously been shown to be polar or

peritrichous in other species, and to our knowledge, a long-axis localization pattern has not previously been reported for any bacterial surface appendage or nanomachine.

Studies on the polarly localized T4P in *Pseudomonas aeruginosa*, a species closely related to the *Acinetobacter* clade and one of the major model systems used to study T4P (*1*), suggest that the chemosensory Pil-Chp system may play a role in controlling which pole of the cell extends T4P (*15*). The Pil-Chp system shares homology to flagellar chemotaxis systems, and in *P. aeruginosa*, the methyl-accepting chemotaxis protein homologue, PilJ, is thought to signal to the CheA homologue, ChpA. The CheW homologue, PilI is thought to act as a scaffold for Pil-Chp signaling, leading to phosphoryl transfer from ChpA to the CheY homologues, PilG and PilH to affect T4P synthesis. To determine whether the Pil-Chp system plays a role in controlling where T4P are synthesized in *A. baylyi*, we made in-frame deletions of all Pil-Chp component genes (Figure 1b). Deletion of *pilG*, *pilI*, and *chpA* all abrogated T4P localization and resulted in the production of peritrichous T4P. However, deletions of *pilH* and, more surprisingly, *pilJ* did not affect T4P patterning, suggesting that another inner membrane component may initiate ChpA phosphoryl transfer in *A. baylyi* (Figure 1c, d). In *P. aeruginosa*, the scaffold protein FimV interacts with the accessory protein FimL to recruit PilG to T4P machinery sites (*16*). Although *A. baylyi* lacks a FimV homologue, deletion of *fimL* also resulted in peritrichous pilus localization (Figure 1c, d). In *P. aeruginosa*, T4P machinery is localized to both poles, but PilG is thought to control which cell pole extends T4P (*17*, *18*). However, an mCherry fusion to the outer membrane secretin, PilQ, in *A. baylyi* demonstrated the same long-axis localization pattern as labeled T4P, revealing a unique function for the Pil-Chp pathway in *A. baylyi* in regulating positioning of T4P machinery and not simply regulating pilus dynamic activity (Supplemental figure 2).

Because PilG shares homology to two-component system response regulators, which drive physiological changes downstream of an input signal, we hypothesized that PilG may control the long-axis positioning of T4P machines. Consistent with this, we found that PilG-mRuby3 localizes to the base of extended T4P (Supplemental figure 3a). Deletions of *pilI* and *chpA* resulted in aberrant PilG-mRuby3 localization, mirroring T4P patterning in those mutants (Figure 1e). The *fimL* mutant displayed

cytoplasmic PilG signal, consistent with FimL playing a role in PilG localization (Figure 1e). Notably, PilG-mRuby3 fluorescence intensity was diminished in mutants with aberrant localization, suggesting a role for the Pil-Chp pathway in controlling PilG levels (Supplemental figure 3b). The percent of cells making T4P in Pil-Chp mutants was largely unchanged, suggesting an additional divergence from *P. aeruginosa* where the Pil-Chp pathway also controls T4P production (*19*) (Supplemental figure 4a).

The Pil-Chp system is homologous to flagellar chemotaxis systems, so we suspected that an external signal may feed into the Pil-Chp pathway to control T4P localization. Outer membrane proteins in Gram-negative bacteria interface with the extracellular environment, and we hypothesized that an outer membrane protein could influence the Pil-Chp system to regulate T4P localization. To test this hypothesis, we deleted several outer membrane proteins containing OmpA-like domains, and found that deletion of the major *ompA* gene, but not others, resulted in peritrichous T4P localization (Figure 1c, d, Supplemental figure 5). Consistent with an external signal feeding into the Pil-Chp pathway through OmpA, PilG-mRuby3 localization in the *ompA* mutant displayed peritrichous localization similar to localization of labeled T4P (Figure 1d, e).

Because *A. baylyi* T4P participate in DNA uptake, we tested whether Pil-Chp mutants with peritrichous localization were impacted for natural transformation. Surprisingly, transformation was unaffected in mutants lacking Pil-Chp components (Supplemental figure 4b). However, incubation of cells with fluorescently-labeled DNA resulted in co-localization of DNA with T4P, which is consistent with the essential role of T4P-DNA binding during natural transformation in *Vibrio cholerae* (*11*) (Figure 2a, Supplemental figure 4b). We reasoned that natural transformation could be used to screen for other factors that regulate T4P in *A. baylyi*. To that end, we performed a high throughput transposon-sequencing screen (Tn-seq) to identify genes required for natural transformation. In this screen, loss of T4P-related genes resulted in negative selection, indicating that they were critical for natural transformation as expected (Figure 2b). To validate our Tn-seq results, we made in-frame deletions of representative genes from each T4P-encoding operon, as well as genes known to be essential for natural transformation that act downstream of T4P. Mutations in the T4P platform protein gene *pilC*, the pilus

regulatory gene *pilY1*, the outer membrane secretin gene *pilQ* and the retraction ATPase gene *pilT* all showed a marked reduction in natural transformation, with most mutants exhibiting transformation rates below our limit of detection (Figure 2c). T4P-labeling of *pilC*, *pilY1*, and *pilQ* mutants revealed no visible T4P fibers (Figure 2d). Mutations in genes that act downstream of T4P, including the periplasmic DNA-binding protein gene *comEA*, the inner membrane DNA-transporter protein gene *comEC*, and the DNA-recombination helicase gene *comM* likewise resulted in a reduction in transformation frequency, however, these strains still produced T4P fibers as expected (Figure 2c, d).

We next sought to determine whether any of the previously uncharacterized genes from our Tn-seq screen reduced natural transformation in *A. baylyi* by affecting T4P activity. Tn-seq revealed that mutations in *pilB*, the canonical extension ATPase gene that is typically co-transcribed with *pilC* and the pre-pilin peptidase, *pilD*, resulted in reduced natural transformation (Figure 2b). However, we also found an additional *pilB* homologue, which we named *pilB2*, that likewise exhibited lower rates of transformation (Figure 2b). Surprisingly, deletion of the canonical *pilB* did not ablate transformation as would be expected based on homology to other T4P (*10*) (Figure 3a). Mutation of *pilB2* only partially reduced transformation; however, natural transformation was undetectable in the *pilB pilB2* double mutant (Figure 3a). T4P labeling in *pilB*, *pilB2*, and *pilB pilB2* mutants revealed that all three mutants were defective in T4P synthesis while *pilT* was intact. Strikingly, a *pilT* deletion, which prevents T4P retraction (*20*), revealed that *pilB* mutant populations had similar numbers of cells producing T4P while *pilB2* mutants were highly defective in T4P synthesis (Figure 3b, c). The *pilB pilB2 pilT* triple mutant produced no detectable T4P fibers (Figure 3b, c). Together, these results indicate that both PilB and PilB2 are essential for efficient T4P extension in *A. baylyi*, with PilB2 playing the dominant role. Phylogenetic analysis of PilB2 homologues found among Gammaproteobacteria (*4*, *21*), which include members of the PilT/VirB11 family of secretion ATPases, revealed that PilB2 clusters with a group of proteins that are phylogenetically distinct from the canonical PilB ATPase (Figure 3d, Supplemental figure 6). PilB and PilB2 proteins are as divergent from one another as PilB and the type II secretion system proteins XcpR/GspE, or PilB and the MshE motors that drive mannose-sensitive haemagglutinin (MSHA) pilus

synthesis, suggesting that PilB2 evolved as a functionally divergent class of proteins that is distinct from canonical PilB extension motors. These results suggest that proteins that cluster with PilB2 may play similar functions in other bacterial species and that multiple extension ATPases may be a common feature of diverse T4P.

In addition to revealing the importance of PilB2 in T4P synthesis, our Tn-seq results also uncovered an uncharacterized transcriptional regulator belonging to the XRE-family of transcriptional repressors that is critical for natural transformation (Figure 2b, Figure 4a). Deletion of this regulator, named *cpiR* for competence pilus inhibition repressor, resulted in a 100-fold reduction in transformation (Figure 4b). We hypothesized that CpiR repressed a factor that inhibits natural transformation. Transcriptional repressors are often transcribed immediately adjacent to the genes they repress. We thus deleted the upstream gene, named *cpiA* for competence pilus inhibition actuator (Figure 4a), and found that transformation frequency was restored in the *cpiR cpiA* double mutant background (Figure 4b). Expression of *cpiA* under the control of an IPTG-inducible promoter (P_{tac}) was sufficient to reduce transformation frequency even in the presence of *cpiR*, further suggesting that CpiR represses *cpiA* transcription. Furthermore, we found that CpiR was sufficient to repress the *cpiA* promoter (using a P_{cpiA}-GFP reporter) in the heterologous host *Vibrio cholerae*, which suggests that CpiR is a direct repressor of P_{cpiA} (Figure 4c). Finally, we found that CpiA protein is only produced in a *cpiR* mutant (Figure 4d). These results demonstrate that under lab conditions, CpiR represses *cpiA* transcription to allow for high rates of natural transformation; however, in the absence of CpiR, CpiA is produced and natural transformation is inhibited ~100-fold.

We next sought to determine the mechanism of transformation inhibition by CpiA. Labeling of T4P in a *cpiR* mutant (when CpiA is expressed) revealed that cells were deficient in T4P synthesis (Figure 4e). This defect was dependent on *cpiA* because piliation was restored in the *cpiR cpiA* double mutant (Figure 4e). Deletion of *pilT* restored T4P synthesis in the *cpiR* mutant (i.e. the *cpiR pilT* double mutant) (Figure 4e, f). This phenotype was reminiscent of the restoration of piliation observed in the *pilB*

pilT double mutant, and we hypothesized that CpiA may regulate natural transformation by inhibiting PilB.

To test this hypothesis, we made *pilB cpiR* and *pilB2 cpiR* double mutants. T4P synthesis was unaffected in *pilB cpiR pilT* (where PilB2 is the sole extension ATPase present), while no T4P were detected in *pilB2 cpiR pilT* (where PilB is the sole extension ATPase present) (Figure 4e, f). The defect in T4P synthesis in the *pilB2 cpiR pilT* strain was restored when *cpiA* was deleted in this background, demonstrating that CpiA acts as a PilB inhibitor to control natural transformation (Figure 4e, f). Transformation frequency assays corroborated these results by demonstrating that deletion of *cpiR* only inhibited transformation in the *pilB2* mutant background (where PilB is the sole extension ATPase) and not the *pilB* mutant background (where PilB2 is the sole extension ATPase) (Figure 4g).

Environmental conditions play an integral role in regulating how bacteria respond to and interact with their surroundings. The novel mechanisms of T4P regulation identified here are likely a reflection of how environmental conditions influence bacterial physiology. Many bacteria use chemotaxis systems to sense and respond to changes in environmental signals (*22*). By homology, an external cue likely controls T4P localization through the Pil-Chp pathway. Indeed, the dependence of T4P localization on the outer membrane protein OmpA supports this idea, as OmpA is a juncture for intracellular components and extracellular media. These data demonstrate a novel role for OmpA in addition to its role in cell envelope integrity and virulence as shown in other *Acinetobacter* species (*23*), highlighting its versatility in adapting to variable environmental contexts. Future work will involve identifying the external signals that feed into the Pil-Chp pathway through OmpA to control localization as well as the molecular mechanism underlying T4P localization and the role it plays in the physiology of *Acinetobacter* species.

The acquisition of the additional extension motor PilB2 and the PilB-specific inhibitory protein CpiA also likely resulted from a need to modulate T4P synthesis under different environmental conditions. Bacteria generally limit T4P synthesis to environments where they provide a selective advantage. For example, in *V. cholerae*, the production of T4a competence pili requires chitin and quorum sensing (*24*), which are environmental conditions where cells are likely to encounter other

bacterial cells for horizontal gene transfer; while the T4b toxin-coregulated (TCP) pili required for intestinal colonization are produced in response to host-specific cues (*25*). In *A. baylyi*, both PilB and PilB2 are required for T4P extension and, consequently, efficient natural transformation. While CpiA is not expressed under laboratory conditions (due to CpiR repression), it is possible that different environmental conditions derepress *cpiA* to decrease pilus activity.

These results establish *A. baylyi* as a new model system to study T4P. By uncovering several unknown mechanisms of T4P regulation, these studies underscore the unexplored versatility and diversity of these ubiquitous systems and further highlight the need for new model species to study T4P biology.

Methods

Bacterial strains and culture conditions

Acinetobacter baylyi strain ADP1 was used throughout this study. For a list of strains used throughout, see Supplementary Table 1. *A. baylyi* cultures were grown at 30 °C in Miller lysogeny broth (LB) medium and on agar supplemented with kanamycin (50 µg/mL), spectinomycin (60 µg/mL), gentamycin (30 µg/mL), and/or chloramphenicol (30 µg/mL), rifampicin (30 µg/mL), and/or streptomycin (10 µg/mL) as appropriate.

Construction of mutant strains

Mutants in *A. baylyi* were made using natural transformation as described previously (*20*). Briefly, mutant constructs were made by splicing-by-overlap (SOE) PCR to stich 1) ~3 kb of the homologous region upstream of the gene of interest, 2) the mutation where appropriate (for deletion by allelic replacement with an antibiotic resistance cassette, or the fusion protein), and 3) the downstream region of homology. For a list of primers used to generate mutants in this study, see Supplementary Table 2. The upstream region was amplified using F1 + R1 primers, and the downstream region was amplified using F2 + R2 primers. All antibiotic resistance (AbR) cassettes were amplified with ABD123 (ATTCCGGGGATCCGTCGAC) and ABD124 (TGTAGGCTGGAGCTGCTTC). Fusion proteins were

amplified using the primers indicated in Supplementary Table 2. In-frame deletions were constructed using F1 + R1 primer pairs to amplify the upstream region and F2 + R2 primer pairs to amplify the downstream region with ~20 bp homology to the remaining region of the downstream region built into the R1 primer and ~20 bp homology to the upstream region built into the F2 primer. SOE PCR reactions were performed using a mixture of the upstream and downstream regions, and middle region where appropriate using F1 + R2 primers. SOE PCR products were added with 50 µl of overnight-grown culture to 450 µl of LB in 2 ml round-bottom microcentrifuge tubes (USA Scientific) and grown at 30 °C rotating on a roller drum for 1-3 hours. For AbR-constructs, transformants were diluted out to 10^{-6} and dribble plated on LB and LB + AbR. For in-frame deletions and protein fusion constructs, after the three-hour incubation, cells were incubated with 10 µl of DNaseI (New England Biolabs) for 5 min at room temperature before 450 µl of LB was added. Transformations were grown for an additional hour before cells were diluted and 100 µl of 10^{-6} dilution was plated on LB plates. In-frame deletions were confirmed by PCR using primers ~150 bp up and downstream of the introduced mutation, and fusions were confirmed by sequencing.

Mutants in *V. cholerae* were made by chitin-induced natural transformation exactly as previously described (*26*, *27*). SOE products were generated exactly as described above. The chromosomally integrated P_{BAD} ectopic expression construct is described in detail in ref (*28*).

Natural transformation assays

Assays were performed exactly as previously described (*29*). Briefly, strains were grown overnight in LB broth at 30°C rolling. Then, ~10^8 cells were subcultured into fresh LB medium and 100 ng of tDNA was added. In this study, a ΔACIAD1551::$Spec^R$ PCR product (with 3kb arms of homology) was used as the tDNA. Reactions were incubated with end-over-end rotation at 30°C for 5 hours and then plated for quantitative culture on spectinomycin plates (to quantify transformants) and on plain LB plates (to quantify total viable counts). Data are reported as the transformation frequency, which is defined as the (CFU/mL of transformants) / (CFU/mL of total viable counts).

Tn-seq Analysis

Transposon mutant libraries of *A. baylyi* were generated by electroporation of cells with pDL1093, a vector that allows for Kan^R mini-Tn10 mutagenesis (*30*, *31*), and plating on kanamycin plates. Approximately 100,000 Tn mutants were scraped off of plates and pooled to generate the input transposon mutant library. This mutant library was then subjected to natural transformation in three separate replicates exactly as described above using three different sources of tDNA: a ΔACIAD1551::$Spec^R$ PCR product, an RpsL K43R (Sm^R) PCR product, or an RpoB PCR product from a spontaneous rifampicin resistant mutant. Following incubation with tDNA, reactions were split and outgrown in selective medium overnight (i.e. with the appropriate antibiotic added to select for transformants = "transformant pool") or grown overnight in nonselective medium (i.e. in plain LB medium = "total pool"). Sequencing libraries of the transposon-genomic junctions were generated for the Illumina platform using HTM-PCR exactly as previously described (*31*, *32*). Sequencing data were mapped to the *V. cholerae* N16961 genome (*33*) and the relative abundance of Tn insertions in all samples was determined on the Galaxy platform (*34*). Comparative analyses for Tn-seq were performed treating the "transformant pool" as the output and the "total pool" as the input to determine genes that were over and underrepresented following selection for transformants. Gene fitness was only assessed if a gene contained at least 1 transposon insertion in at least two out of the three replicates of the "total pool" samples. Also, the normalized abundance of insertions within a gene had to be greater than 0.01 in the "total pool" when averaged across all three replicates (where 1 is the expected normalized abundance for a "neutral" gene). These cutoffs allowed us to assess the phenotype of ~83% of the genes (2747/3310) in the *A. baylyi* ADP1 genome. For visualization, the relative abundance of Tn insertions within each gene is plotted from the "transformant pool" relative to the "total pool".

Pilin labeling, imaging, and quantification

Pilin labeling was performed as described previously with some changes (*2*, *3*). Briefly, 100 µl of overnight-grown cultures was added to 900 µl of LB in 1.5 ml microcentrifuge tube, and cells were grown

at 30 °C rotating on a roller drum for 70 min. Cells were then centrifuged at 18,000 x *g* for 1 min and then resuspended in 50 µl of LB before labeling with 25 µg/ml of AlexaFluor488 C_5-maleimide (AF488-mal) (ThermoFisher) for 15 min at room temperature. Labeled cells were centrifuged, washed once with 100 µl of LB without disrupting the pellet, and resuspended in 5-20 µl LB. Cell bodies were imaged using phase contrast microscopy while labeled pili were imaged using fluorescence microscopy on a Nikon Ti-2 microscope using a Plan Apo 100X objective, an FITC filter cube for pili, an mCherry filter cube for mRuby3 and mCherry fusions, a Hamamatsu ORCAFlash4.0 camera, and Nikon NIS Elements Imaging Software. Cell numbers and the percent of cells making pili were quantified manually using ImageJ (*35*). Cells were considered to have "mislocalized pili" if at least two pili were on opposing sides of the cell. All imaging was performed under 1% UltraPure agarose (Invitrogen) pads made with phosphate-buffered saline (PBS) solution.

Western blotting

Western blot analysis was performed exactly as previously described (*36*). Briefly, cells from overnight cultures were concentrated to an OD_{600} of 20. Then, cells were lysed on a FastPrep-24 classic instrument at 4°C, and then clarified by centrifugation. Lysates were then mixed with an equal volume of 2× SDS-PAGE sample buffer (220 mM Tris, pH 6.8, 25% glycerol, 1.2% SDS, 0.02% bromophenol blue, and 5% β-mercaptoethanol) and boiled. Proteins were separated on a 15% SDS polyacrylamide gel by SDS electrophoresis, electrophoretically transferred to a polyvinylidene difluoride (PVDF) membrane, and probed with rabbit polyclonal α-FLAG antibodies (Sigma Aldrich) or mouse monoclonal α-RpoA (BioLegend) primary antibodies. Blots were then incubated with α-rabbit or α-mouse horseradish peroxidase (HRP)-conjugated secondary antibodies, developed using Pierce ECL Western blotting substrate (Thermo Fisher), and imaged on a Protein Simple FluorChem E instrument.

Measuring GFP fluorescence in reporter strains

V. cholerae reporter strains harboring P_{cpiA}-GFP were grown to late log in LB medium with or without 0.2% arabinose as indicated. Cells were then washed once in instant ocean medium (7g/L; Aquarium Systems) and transferred to a 96-well plate. Fluorescence was then determined on a Biotek H1M plate reader with monochromater set to 500 nm for excitation and 540 nm for emission.

Fluorescent DNA binding/uptake

A ~7 kb PCR product was fluorescently labeled as described previously (*11*) using the Cy3 LabelIT kit (Mirus Biosciences) as per manufacturer recommendations. For the parent strain, 1 µl (100 ng) of Cy3-DNA was added to 900 µl of LB in a 1.5 ml microcentrifuge tube along with 100 µl of overnight-grown cultures, and cells were grown at 30°C rotating on a roller drum for 70 min. Pili were then labeled as described above.

To visualize DNA-binding in the *pilT* mutant, cells were grown as described above, but 1 µl (100 ng) of Cy3-DNA was added to cells along with AF488-mal and incubated for 25 min before washing. Cells were imaged using the same microscopy setup described above, using a dsRed filter cube to image Cy3-DNA.

Phylogenetic analysis

PilB2 homologues were identified by BLAST using 43 manually selected Gammaproteobacteria genomes (*37*) through Integrated Microbial Genomes and Microbiomes online resources (IMG) (*38*) resulting in 209 protein sequences. The FtsK protein from *A. baylyi* ADP1 was added and used as an outgroup. Through the NGPhylogeny.fr server (*39*), sequences were aligned using the default parameters of MAFFT (*40*), and phylogenetic tree construction was performed on the aligned sequences using the default parameters of FastTree software (*41*, *42*) set to perform 100 bootstraps (*43*). The resulting tree was visualized using the Interactive Tree of Life (iTOL) visualization software (*44*), from which trees were exported for publication.

Acknowledgements: We would like to thank E. Geisinger for *A. baylyi* ADP1 ATCC33305 wildtype strain, and we would like to thank K. Hummels and B. Bratton for helpful suggestions on phylogenetic analysis. CKE is a Damon Runyon Fellow supported by the Damon Runyon Cancer Research Foundation (DRG-2385-20). This work was supported in part by the National Science Foundation, through the Center for the Physics of Biological Function (PHY-1734030). This work was supported by grant R35GM128674 from the National Institutes of Health awarded to ABD and the National Institutes of Health Pioneer Award 1DP1AI124669-01 awarded to ZG.

Author contributions: CKE and ABD designed and coordinated the overall study. CKE, TND, CAK and ABD performed the experiments. All authors analyzed and interpreted data. CKE and ABD wrote the manuscript with help from ZG and JWS.

Competing interests: The authors declare no competing interests.

Data availability statement: The data that support the findings of this study are available from the corresponding authors upon request.

References

1. L. L. Burrows, Pseudomonas aeruginosa twitching motility: type IV pili in action. *Annu Rev Microbiol*. **66**, 493–520 (2012).
2. C. K. Ellison, J. Kan, R. S. Dillard, D. T. Kysela, A. Ducret, C. Berne, C. M. Hampton, Z. Ke, E. R. Wright, N. Biais, A. B. Dalia, Y. V. Brun, Obstruction of pilus retraction stimulates bacterial surface sensing. *Science* **358**, 535–538 (2017).
3. C. K. Ellison, T. N. Dalia, A. B. Dalia, Y. V. Brun, Real-time microscopy and physical perturbation of bacterial pili using maleimide-conjugated molecules. *Nat. Protoc.* **14** (2019), doi:10.1038/s41596-019-0162-6.
4. R. Denise, S. S. Abby, E. P. C. Rocha, Diversification of the type IV filament superfamily into machines for adhesion, protein secretion, DNA uptake, and motility. *PLOS Biol.* **17**, e3000390 (2019).
5. L. Craig, K. T. Forest, B. Maier, Type IV pili: dynamics, biophysics and functional consequences. *Nat. Rev. Microbiol.*, 1 (2019).
6. A. J. Merz, M. So, M. P. Sheetz, Pilus retraction powers bacterial twitching motility. *Nature*. **407**, 98–102 (2000).
7. R. A. Snyder, C. K. Ellison, G. B. Severin, G. B. Whitfield, C. M. Waters, Y. V. Brun, Surface sensing stimulates cellular differentiation in Caulobacter crescentus. *Proc. Natl. Acad. Sci.* (2020), doi:10.1073/PNAS.1920291117.
8. A. Siryaporn, S. L. Kuchma, G. A. O'Toole, Z. Gitai, G. A. O'Toole, Z. Gitai, Surface attachment induces Pseudomonas aeruginosa virulence. *Proc. Natl. Acad. Sci.* **111**, 16860–16865 (2014).
9. A. Persat, Y. F. Inclan, J. N. Engel, H. A. Stone, Z. Gitai, Type IV pili mechanochemically regulate virulence factors in *Pseudomonas aeruginosa*. *Proc. Natl. Acad. Sci.* **112**, 7563–7568 (2015).
10. P. Seitz, M. Blokesch, DNA-uptake machinery of naturally competent Vibrio cholerae. *Proc. Natl. Acad. Sci. U. S. A.* **110**, 17987–92 (2013).

11. C. K. Ellison, T. N. Dalia, A. Vidal Ceballos, J. C.-Y. Wang, N. Biais, Y. V. Brun, A. B. Dalia, Retraction of DNA-bound type IV competence pili initiates DNA uptake during natural transformation in Vibrio cholerae. *Nat. Microbiol.* **3**, 773–780 (2018).

12. C. M. Harding, E. N. Tracy, M. D. Carruthers, P. N. Rather, L. A. Actis, R. S. Munson, Acinetobacter baumannii strain M2 produces type IV Pili which play a role in natural transformation and twitching motility but not surface-associated motility. *MBio*. **4** (2013), doi:10.1128/mBio.00360-13.

13. A. S. Godeux, A. Lupo, M. Haenni, S. Guette-Marquet, G. Wilharm, M. H. Laaberki, X. Charpentier, Fluorescence-based detection of natural transformation in drug-resistant acinetobacter baumannii. *J. Bacteriol.* **200** (2018), doi:10.1128/JB.00181-18.

14. D. Metzgar, J. M. Bacher, V. Pezo, J. Reader, V. Döring, P. Schimmel, P. Marlière, V. de Crécy-Lagard, Acinetobacter sp. ADP1: An ideal model organism for genetic analysis and genome engineering. *Nucleic Acids Res.* **32**, 5780–5790 (2004).

15. R. Jain, O. Sliusarenko, B. I. Kazmierczak, Interaction of the cyclic-di-GMP binding protein FimX and the Type 4 pilus assembly ATPase promotes pilus assembly. *PLOS Pathog.* **13**, e1006594 (2017).

16. Y. F. Inclan, A. Persat, A. Greninger, J. Von Dollen, J. Johnson, N. Krogan, Z. Gitai, J. N. Engel, A scaffold protein connects type IV pili with the Chp chemosensory system to mediate activation of virulence signaling in Pseudomonas aeruginosa. *Mol. Microbiol.* **101**, 590–605 (2016).

17. J. J. Bertrand, J. T. West, J. N. Engel, Genetic analysis of the regulation of type IV pilus function by the Chp chemosensory system of Pseudomonas aeruginosa. *J. Bacteriol.* **192**, 994–1010 (2010).

18. T. Carter, R. N. C. Buensuceso, S. Tammam, R. P. Lamers, H. Harvey, P. L. Howell, L. L. Burrows, The type IVa pilus machinery is recruited to sites of future cell division. *MBio*. **8** (2017), doi:10.1128/mBio.02103-16.

19. R. N. C. Buensuceso, M. Daniel-Ivad, S. L. N. Kilmury, T. L. Leighton, H. Harvey, P. L. Howell, L. L. Burrowsa, Cyclic AMP-independent control of twitching motility in Pseudomonas

aeruginosa. *J. Bacteriol.* **199** (2017), doi:10.1128/JB.00188-17.

20. J. L. Chlebek, H. Q. Hughes, A. S. Ratkiewicz, R. Rayyan, J. C.-Y. Wang, B. E. Herrin, T. N. Dalia, N. Biais, A. B. Dalia, PilT and PilU are homohexameric ATPases that coordinate to retract type IVa pili. *PLOS Genet.* **15**, e1008448 (2019).

21. M. McCallum, S. Tammam, A. Khan, L. L. Burrows, P. L. Howell, The molecular mechanism of the type IVa pilus motors. *Nat. Commun.* **8**, 15091 (2017).

22. G. H. Wadhams, J. P. Armitage, Making sense of it all: Bacterial chemotaxis. *Nat. Rev. Mol. Cell Biol.* **5** (2004), pp. 1024–1037.

23. J. A. Gaddy, A. P. Tomaras, L. A. Actis, The Acinetobacter baumannii 19606 OmpA protein plays a role in biofilm formation on abiotic surfaces and in the interaction of this pathogen with eukaryotic cells. *Infect. Immun.* **77**, 3150–3160 (2009).

24. K. L. Meibom, M. Blokesch, N. A. Dolganov, C.-Y. Wu, G. K. Schoolnik, Chitin Induces Natural Competence in Vibrio cholerae. *Science (80-.).* **310**, 1824–1827 (2005).

25. D. A. Schuhmacher, K. E. Klose, Environmental signals modulate ToxT-dependent virulence factor expression in Vibrio cholerae. *J. Bacteriol.* **181**, 1508–1514 (1999).

26. A. B. Dalia, E. McDonough, A. Camilli, Multiplex genome editing by natural transformation. *Proc. Natl. Acad. Sci. U. S. A.* **111**, 8937–42 (2014).

27. A. B. Dalia, in *Methods in molecular biology (Clifton, N.J.)* (2018; http://www.ncbi.nlm.nih.gov/pubmed/30047054), vol. 1839, pp. 53–64.

28. T. N. Dalia, J. L. Chlebek, A. B. Dalia, *bioRxiv*, in press, doi:10.1101/2020.03.02.973776.

29. T. M. Nero, T. N. Dalia, J. C. Y. Wang, D. T. Kysela, M. L. Bochman, A. B. Dalia, ComM is a hexameric helicase that promotes branch migration during natural transformation in diverse Gram-negative species. *Nucleic Acids Res.* **46**, 6099–6111 (2018).

30. L. M. Shull, A. Camilli, in *Methods in Molecular Biology* (Humana Press Inc., 2018), vol. 1839, pp. 103–116.

31. E. Mcdonough, D. W. Lazinski, A. Camilli, Identification of in vivo regulators of the Vibrio

choleraexds gene using a high-throughput genetic selection. *Mol. Microbiol.* **92**, 302–315 (2014).

32. D. W. Lazinski, A. Camilli, Homopolymer tail-mediated ligation PCR: A streamlined and highly efficient method for DNA cloning and library construction. *Biotechniques*. **54**, 25–34 (2013).

33. J. F. Heidelberg, J. A. Elsen, W. C. Nelson, R. A. Clayton, M. L. Gwinn, R. J. Dodson, D. H. Haft, E. K. Hickey, J. D. Peterson, L. Umayam, S. R. Gill, K. E. Nelson, T. D. Read, H. Tettelin, D. Richardson, M. D. Ermolaeva, J. Vamathevan, S. Bass, Q. Halving, I. Dragol, P. Sellers, L. McDonald, T. Utterback, R. D. Fleishmann, W. C. Nierman, O. White, S. L. Saizberg, H. O. Smith, R. R. Colwell, J. J. Mekalanos, C. J. Venter, C. M. Fraser, DNA sequence of both chromosomes of the cholera pathogen Vibrio cholerae. *Nature*. **406**, 477–483 (2000).

34. E. Afgan, D. Baker, M. van den Beek, D. Blankenberg, D. Bouvier, M. Čech, J. Chilton, D. Clements, N. Coraor, C. Eberhard, B. Grüning, A. Guerler, J. Hillman-Jackson, G. Von Kuster, E. Rasche, N. Soranzo, N. Turaga, J. Taylor, A. Nekrutenko, J. Goecks, The Galaxy platform for accessible, reproducible and collaborative biomedical analyses: 2016 update. *Nucleic Acids Res.* **44**, W3–W10 (2016).

35. C. A. Schneider, W. S. Rasband, K. W. Eliceiri, NIH Image to ImageJ: 25 years of image analysis. *Nat. Methods*. **9**, 671–675 (2012).

36. C. Klancher, J. Newman, A. Ball, J. van Kessel, A. Dalia, Species-specific quorum sensing represses the chitobiose utilization locus in Vibrio cholerae. *Appl. Environ. Microbiol.* **86** (2020), doi:10.1128/AEM.00915-20.

37. S. Mukherjee, D. Stamatis, J. Bertsch, G. Ovchinnikova, H. Y. Katta, A. Mojica, I. M. A. Chen, N. C. Kyrpides, T. B. K. Reddy, Genomes OnLine database (GOLD) v.7: Updates and new features. *Nucleic Acids Res.* **47**, D649–D659 (2019).

38. I. M. A. Chen, K. Chu, K. Palaniappan, M. Pillay, A. Ratner, J. Huang, M. Huntemann, N. Varghese, J. R. White, R. Seshadri, T. Smirnova, E. Kirton, S. P. Jungbluth, T. Woyke, E. A. Eloe-Fadrosh, N. N. Ivanova, N. C. Kyrpides, IMG/M v.5.0: An integrated data management and comparative analysis system for microbial genomes and microbiomes. *Nucleic Acids Res.* **47**,

D666–D677 (2019).

39. F. Lemoine, D. Correia, V. Lefort, O. Doppelt-Azeroual, F. Mareuil, S. Cohen-Boulakia, O. Gascuel, NGPhylogeny.fr: New generation phylogenetic services for non-specialists. *Nucleic Acids Res.* **47**, W260–W265 (2019).

40. K. Katoh, D. M. Standley, MAFFT multiple sequence alignment software version 7: Improvements in performance and usability. *Mol. Biol. Evol.* **30**, 772–780 (2013).

41. M. N. Price, P. S. Dehal, A. P. Arkin, Fasttree: Computing large minimum evolution trees with profiles instead of a distance matrix. *Mol. Biol. Evol.* **26**, 1641–1650 (2009).

42. M. N. Price, P. S. Dehal, A. P. Arkin, FastTree 2 - Approximately maximum-likelihood trees for large alignments. *PLoS One*. **5**, e9490 (2010).

43. F. Lemoine, J. B. Domelevo Entfellner, E. Wilkinson, D. Correia, M. Dávila Felipe, T. De Oliveira, O. Gascuel, Renewing Felsenstein's phylogenetic bootstrap in the era of big data. *Nature*. **556**, 452–456 (2018).

44. I. Letunic, P. Bork, Interactive Tree of Life (iTOL) v4: Recent updates and new developments. *Nucleic Acids Res.* **47**, W256–W259 (2019).

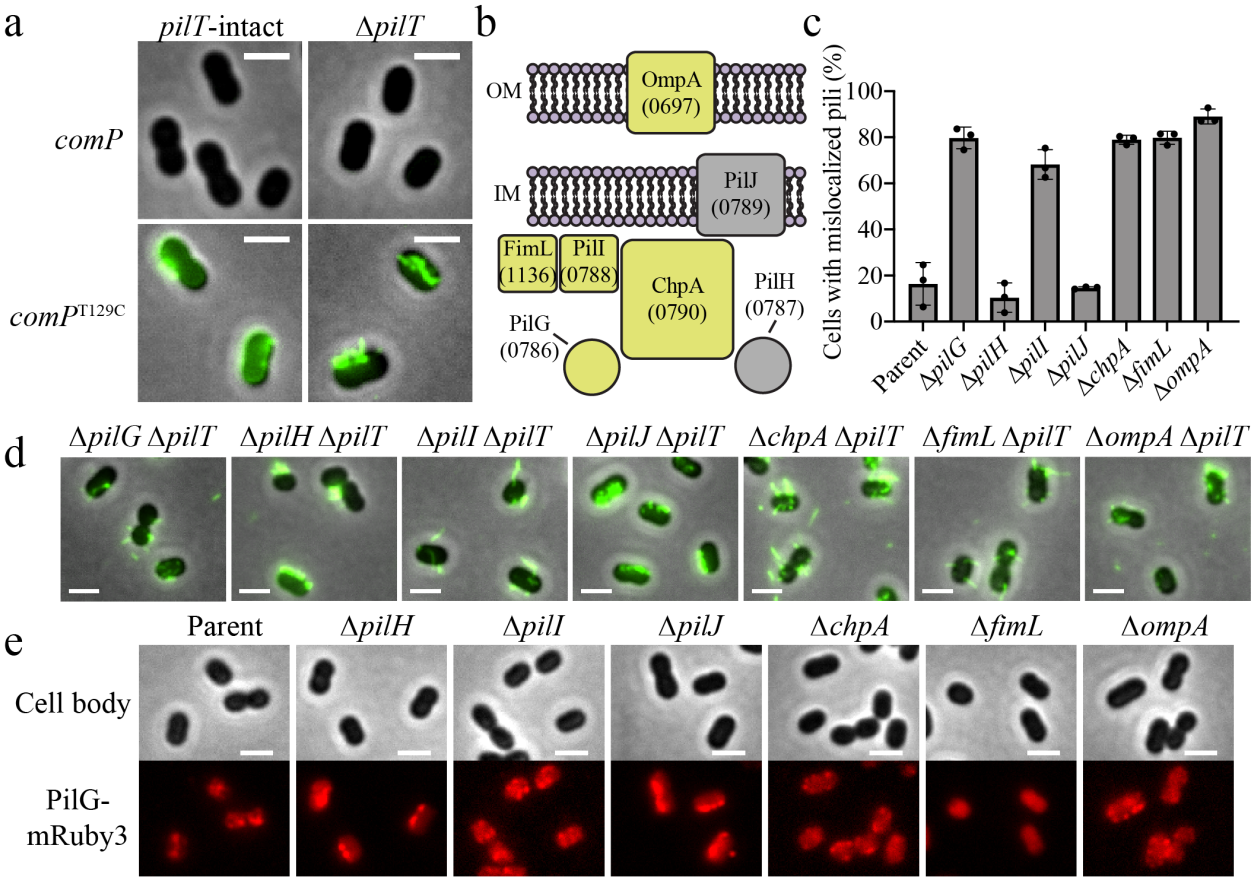

Figure 1. *A. baylyi* T4aP are produced in a line along the long axis of the cell body in a Pil-Chp dependent manner. (**a**) Representative images of indicated strains labeled with AF488-mal. (**b**) Schematic of the *A. baylyi* components of the Pil-Chp system. Deletion of tan proteins alters T4P localization, while deletion of the gray proteins does not. Numbers in parentheses are the ACIAD gene designations for each component. OM, outer membrane; IM, inner membrane. (**c**) Percent of piliated cells in *pilT* mutants with mislocalized T4P in indicated strains. Cells were determined to have "mislocalized pili" if they had at least two pili on opposing sides of the long axis of the cell body. Cells that only made one pilus were counted in the total number of piliated cells but were not counted as "mislocalized." Each data point represents an independent, biological replicate and bar graphs indicate the mean ± SD. For each biological replicate, a minimum of 70 total cells were assessed. (**d**) Representative images of indicated strains labeled with AF488-mal with background fluorescence subtracted. (**e**) Representative images of

indicated PilG-mRuby3 strains with background fluorescence subtracted and fluorescence channel lookup tables adjusted to show PilG-mRuby3 localization. Scale bars, 2 μm.

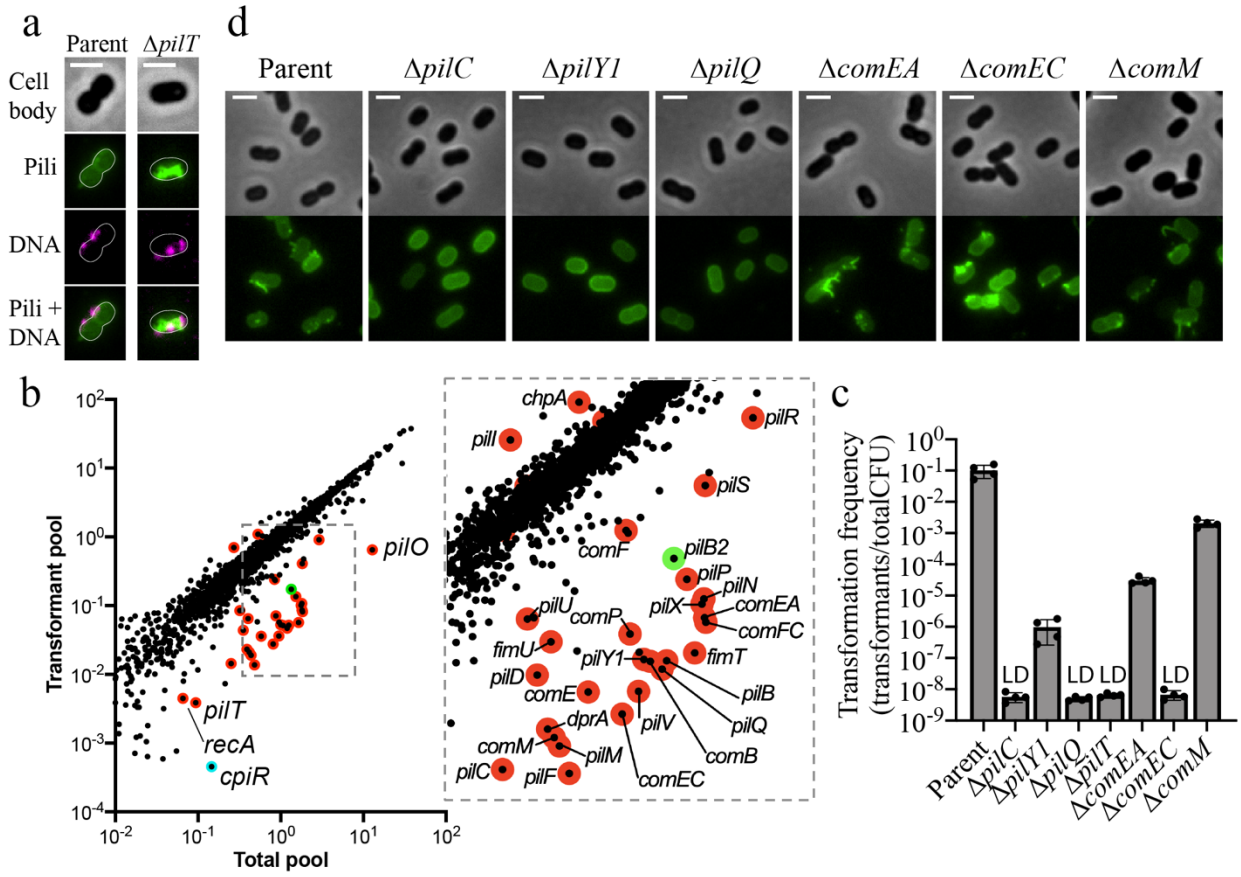

Figure 2. Tn-seq reveals factors important for natural transformation and T4P synthesis. (**a**) Representative images of cells with AF488-mal labeled pili incubated with fluorescently-labeled DNA. (**b**) Visual representation of Tn-seq screen showing the relative abundance of each gene in the "total pool" of transposon mutants compared to the "transformant pool" recovered after natural transformation. Known T4P regulatory genes are outlined in red. *pilB2* is outlined in green, and *cpiR* is outlined in cyan. (**c**) Natural transformation assays of indicated strains. Each data point represents a biological replicate and bar graphs indicate the mean ± SD. LD, limit of detection. (**d**) Representative images of strains from natural transformation assays shown in **c** labeled with AF488-mal. Scale bars, 2 µm.

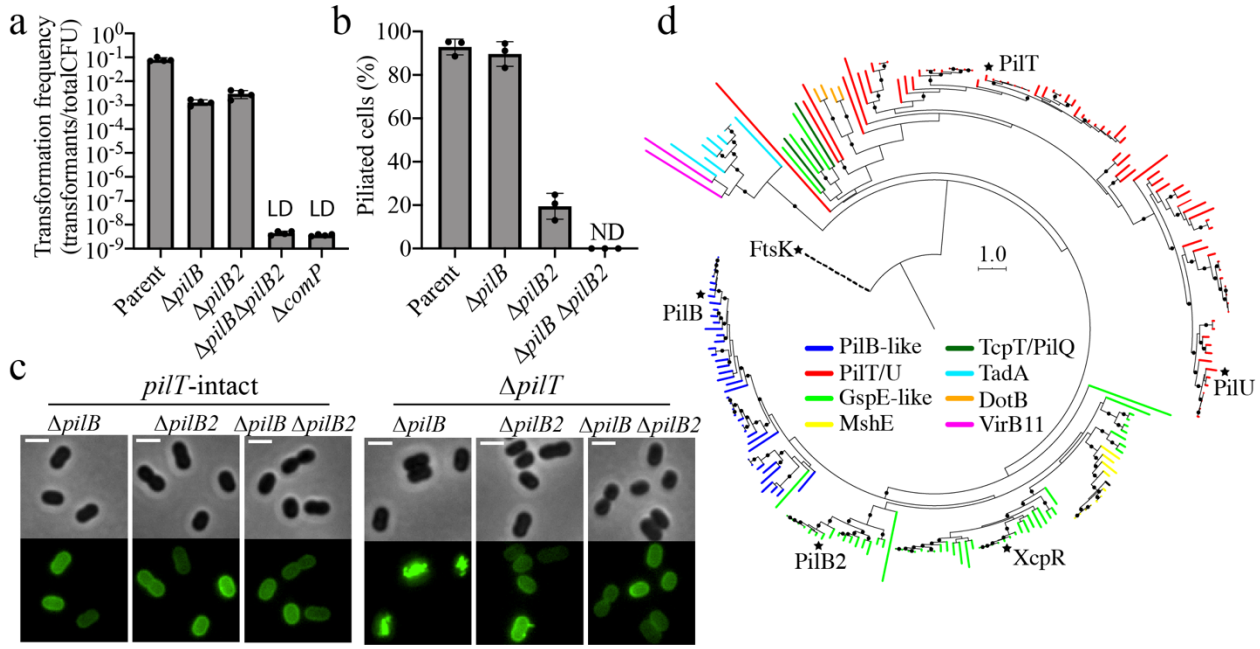

Figure 3. PilB2 is a phylogenetically distinct PilB homologue that is required for efficient T4P extension in *A. baylyi*. (**a**) Natural transformation assays of indicated strains. Each data point represents a biological replicate and bar graphs indicate the mean ± SD. LD, limit of detection. (**b**) Percent of piliated cells in *pilT* mutant populations of indicated strains. Each data point represents an independent, biological replicate and bar graphs indicate the mean ± SD. For each biological replicate, a minimum of 70 total cells were assessed. ND, no pili detected. (**c**) Representative images of indicated strains labeled with AF488-mal with background fluorescence subtracted. Scale bars, 2 µm. (**d**) A rooted phylogeny of PilB2 homologues found among Gammaproteobacteria. Branches are colored according to protein annotations in IMG, and nodes with boostrap values greater than or equal to 70% are indicated by black circles. Black stars are at the tips of branches representing *A. baylyi* proteins with indicated protein names.

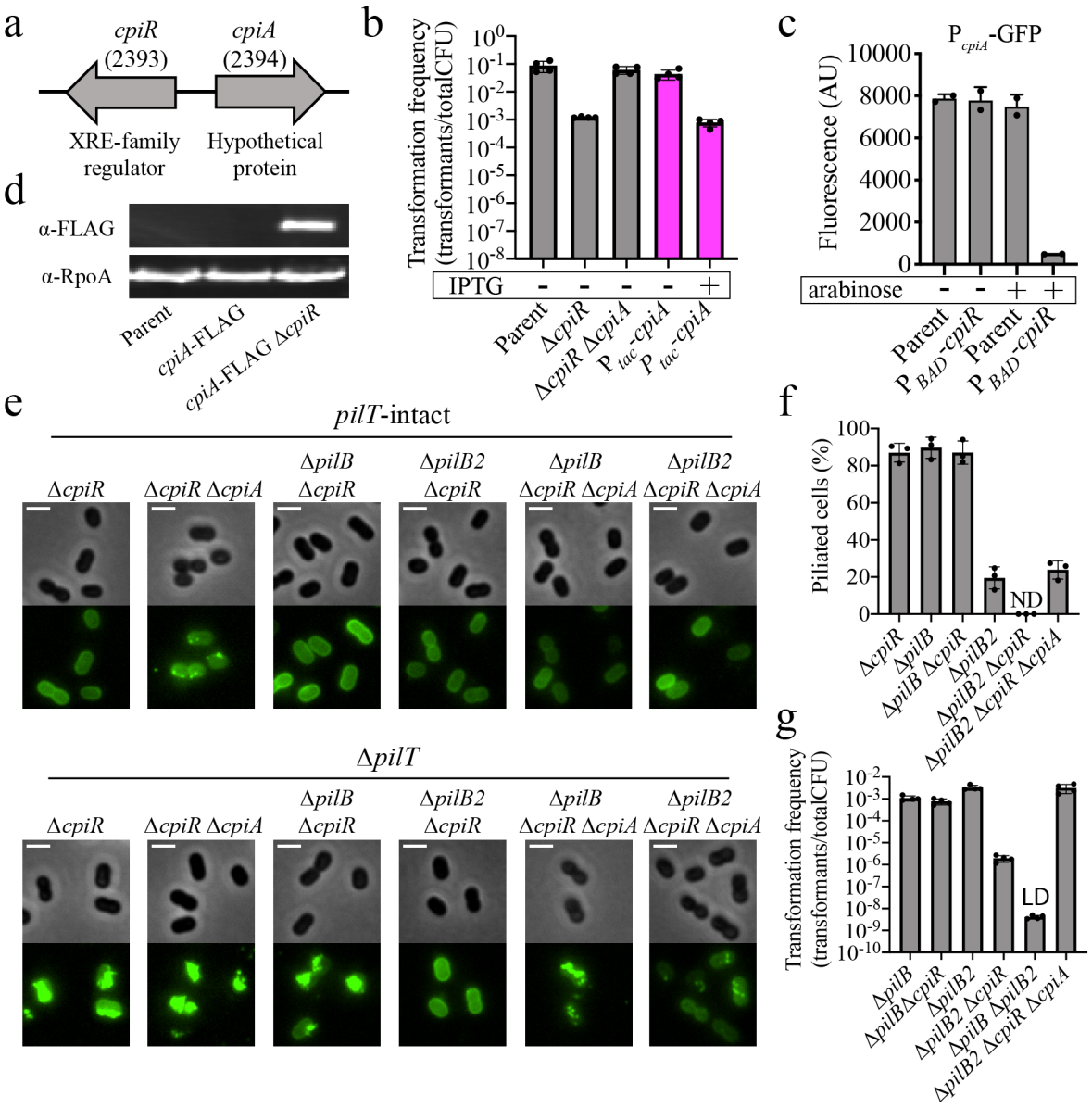

Figure 4. *A. baylyi* T4P extension is regulated by the PilB-inhibitor protein, CpiA, whose expression is controlled by the transcriptional repressor, CpiR. (**a**) Schematic *cpiRA* locus organization. (**b**) Natural transformation assays of the indicated strains performed with or without 100 µM IPTG added as indicated. Each data point represents a biological replicate and bar graphs indicate the mean ± SD. Pink bars denote a strain where *cpiA* is expressed at an ectopic location under the control of an IPTG-inducible promoter. (**c**) Fluorescence intensity of *V. cholerae* strains harboring a P_{cpiA}-GFP reporter and a P_{BAD}-*cpiR* ectopic expression construct as indicated when grown with or without 0.2% arabinose as indicated. Each

data point represents a biological replicate and bar graphs indicate the mean ± SD. (**d**) Western blot showing CpiA-FLAG production in the indicated strains. RpoA was detected as a loading control. (**e**) Representative images of indicated strains labeled with AF488-mal with background fluorescence subtracted. Scale bars, 2 µm. (**f**) Percent of piliated cells in *pilT* mutant populations of indicated strains. Each data point represents an independent, biological replicate and bar graphs indicate the mean ± SD. For each biological replicate, a minimum of 70 total cells were assessed. ND, no pili detected. (**g**) Natural transformation assays of indicated strains. Each data point represents a biological replicate and bar graphs indicate the mean ± SD. LD, limit of detection.

Supplementary Materials for:

Novel mechanisms of type IV pilus regulation in *Acinetobacter baylyi*

Courtney K. Ellison[1,2*], Triana N. Dalia[3], Catherine A. Klancher[3], Joshua W. Shaevitz[1*], Zemer Gitai[2*], and Ankur B. Dalia[3*]

1. Lewis-Sigler Institute for Integrative Genomics, Princeton University, Princeton, NJ
2. Department of Molecular Biology, Princeton University, Princeton, NJ
3. Department of Biology, Indiana University, Bloomington, IN

*Correspondence to: c.ellison@princeton.edu, shaevitz@princeton.edu, zgitai@princeton.edu, ankdalia@indiana.edu

This file includes:

Supplementary Figures 1-6

Supplementary Tables 1-2

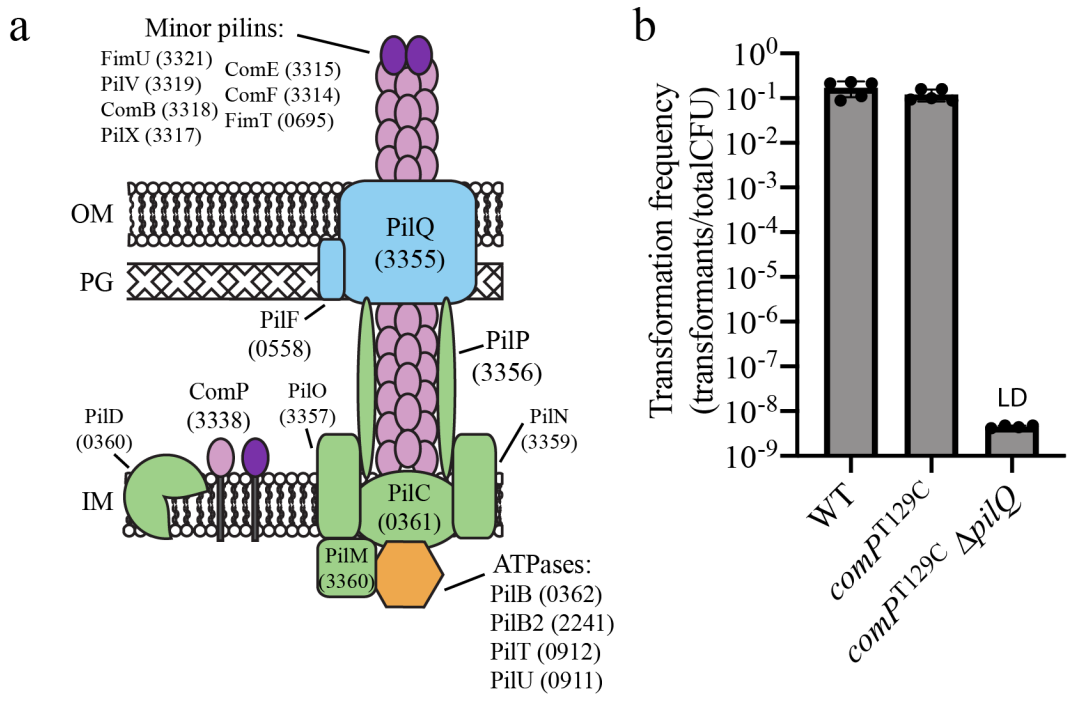

Supplemental figure 1. The strain for labeling T4P in *A. baylyi* is fully functional. (a) Schematic of assembled T4P components found in *A. baylyi*. Numbers in parentheses are ACIAD numbers associated with each component. OM, outer membrane; PG, peptidoglycan; IM, inner membrane. (b) Natural transformation assays of indicated strains. Each data point represents a biological replicate and bar graphs indicate the mean ± SD. The transformation frequency of the Δ*pilQ* strain was below the limit of detection, indicated by LD.

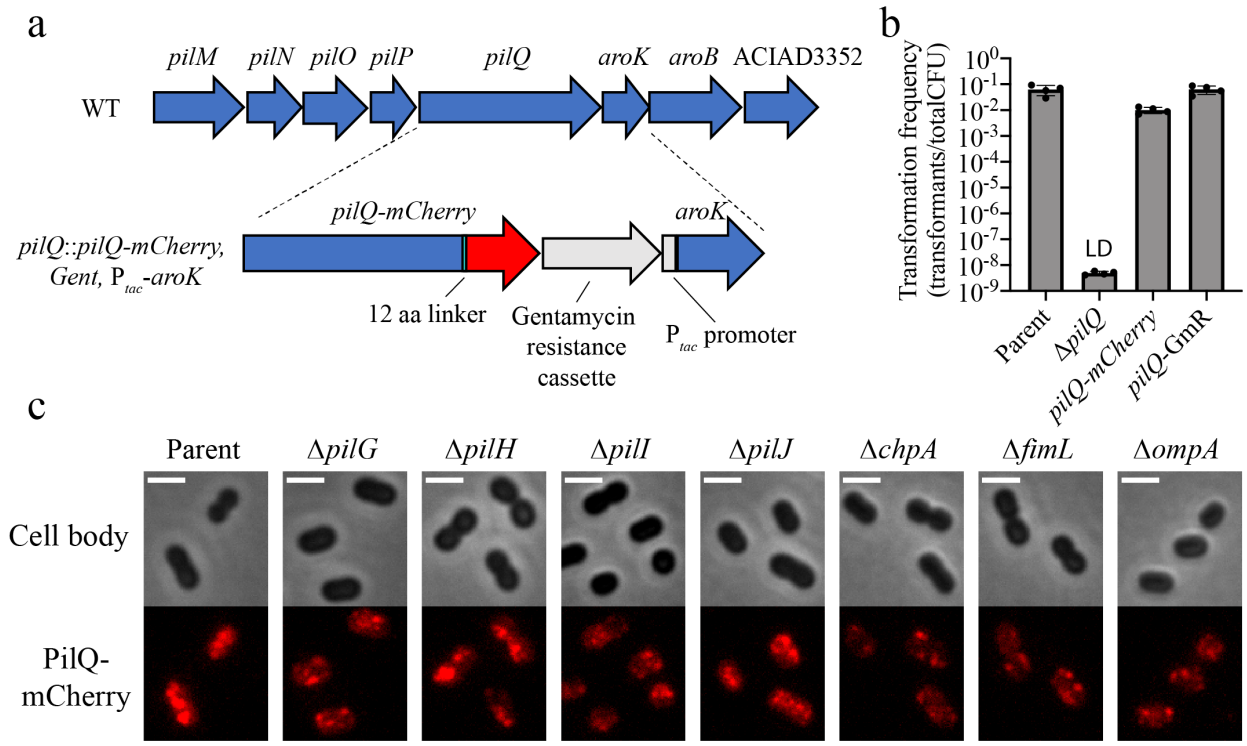

Supplemental figure 2. PilQ-mCherry localizes to the long-axis of the cell dependent on components of the Pil-Chp pathway. (a) Schematic of *pilQ-mCherry* gene locus. Attempts to make *pilQ-mCherry* by natural transformation without a selective marker were unsuccessful, and we thus added a gentamycin resistance cassette downstream of *pilQ*. Because *pilQ* is in an operon with the essential gene *aroK* immediately downstream, we added a constitutively active P_{tac} promoter to drive *aroK* expression. (b) Natural transformation assays of indicated strains. The *pilQ*-GmR control strain contains the same GmR-P_{tac} marker downstream of PilQ present in *pilQ-mCherry*, but PilQ is untagged in this background. Each data point represents a biological replicate and bar graphs indicate the mean ± SD. The transformation frequency of the Δ*pilQ* strain was below the limit of detection, indicated by LD. (c) Representative images of indicated PilQ-mCherry strains with background fluorescence subtracted. Scale bars, 2 µm.

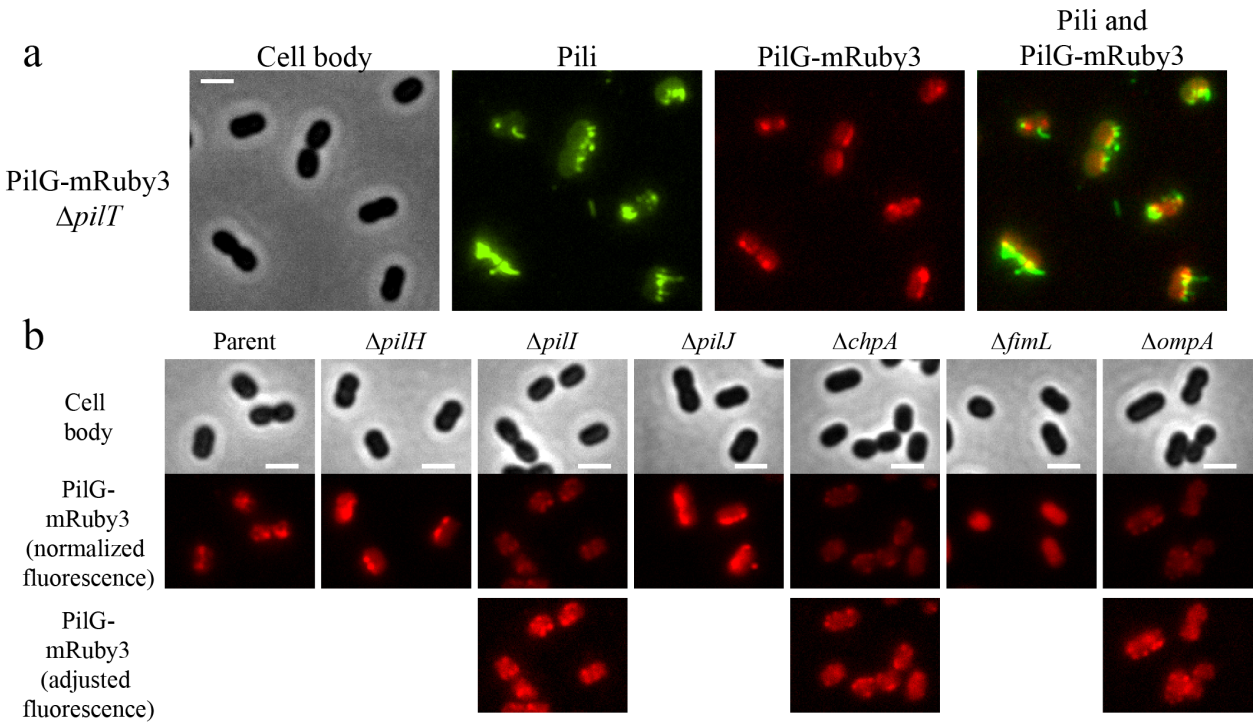

Supplemental figure 3. PilG-mRuby3 localizes at the base of T4P, and its expression is reduced in Pil-Chp mutants. (a) Representative image of PilG-mRuby3 Δ*pilT* strain labeled with AF488-mal with background fluorescence subtracted. (b) Representative images of PilG-mRuby3 localization in indicated strains with background fluorescence subtracted. Images in (b) are identical to images shown in Figure 1e, except with altered fluorescence lookup tables (LUT). Normalized fluorescence images have the same fluorescence LUT across strains, while adjusted fluorescence images have LUTs adjusted for protein visibility to show PilG-mRuby3 localization patterns. Scale bars, 2 μm.

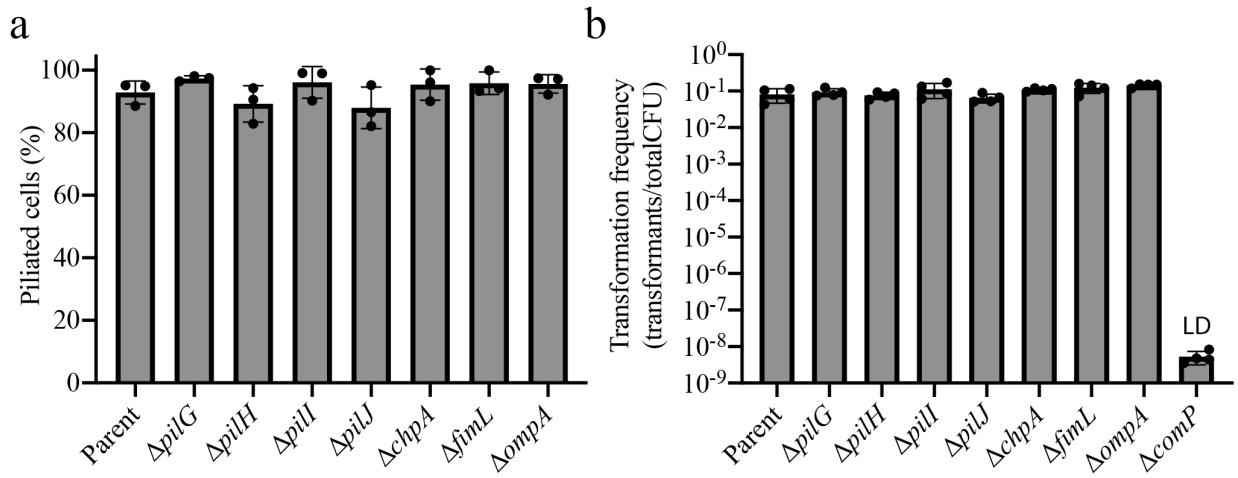

Supplemental figure 4. Pil-Chp mutants are unimpaired in T4P synthesis and are not required for natural transformation. (a) Percent of piliated cells in *pilT* mutant populations of indicated strains. Each data point represents an independent, biological replicate and bar graphs indicate the mean ± SD. For each biological replicate, a minimum of 70 total cells were assessed. (b) Natural transformation assays of indicated strains. Each data point represents a biological replicate and bar graphs indicate the mean ± SD. The transformation frequency of the Δ*comP* strain was below the limit of detection, indicated by LD.

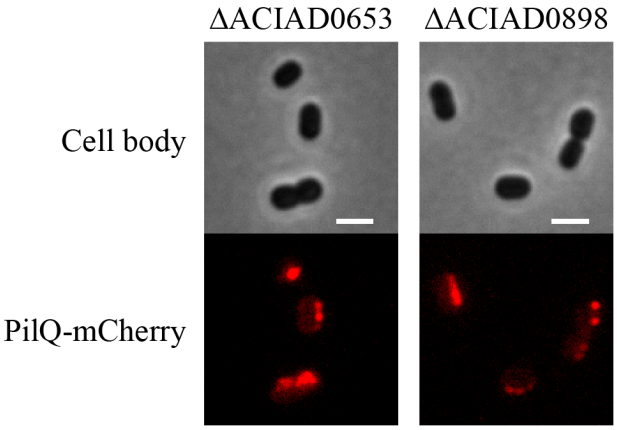

Supplemental figure 5. Other OmpA domain-containing proteins do not affect pilus machinery localization. Representative images of indicated PilQ-mCherry strains with background fluorescence subtracted. Scale bars, 2 μm.

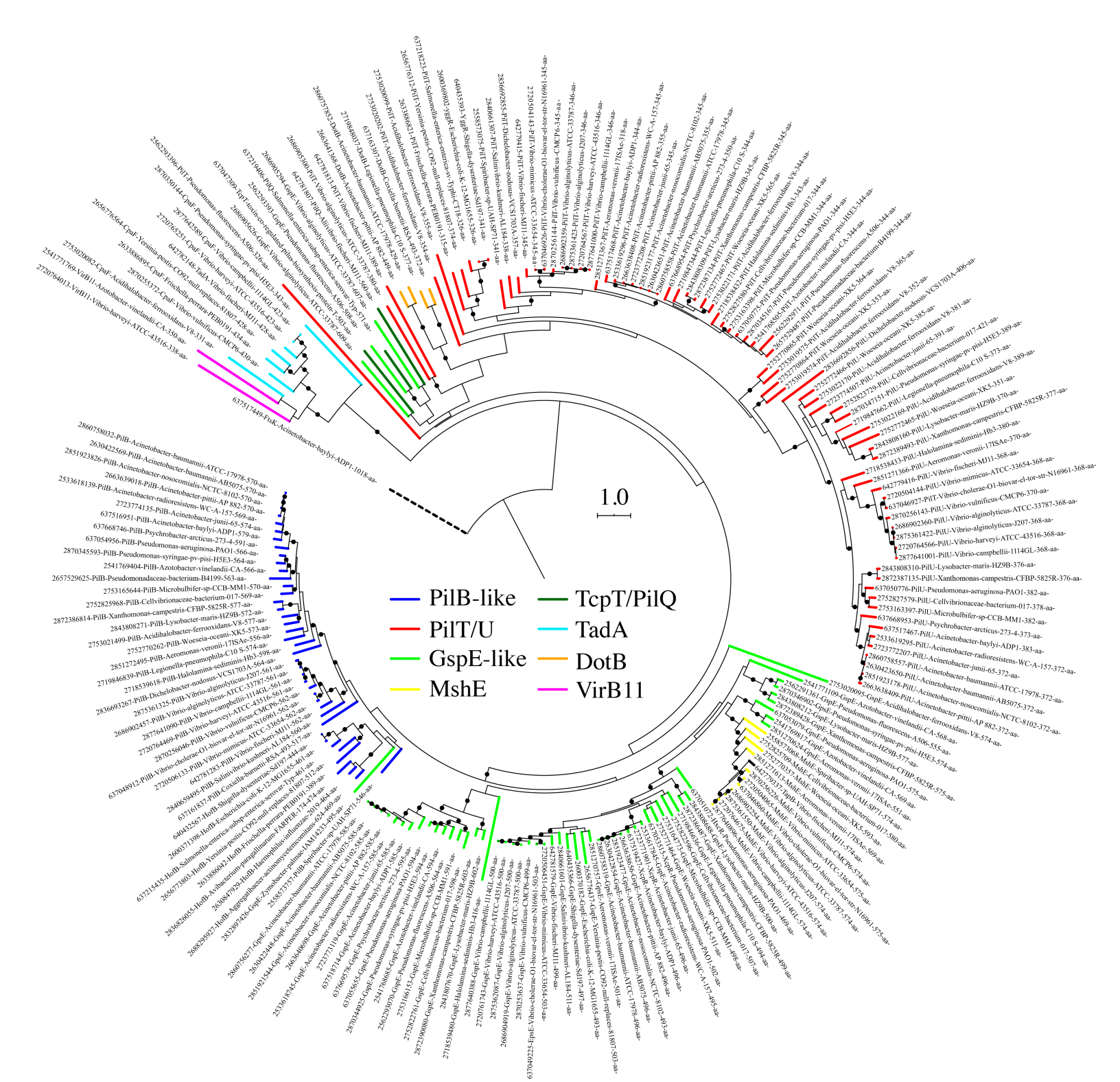

Supplemental figure 6. PilB2 clusters with a group of other GspE-like proteins that are distinct from PilB proteins. A rooted phylogeny of PilB2 homologues shown in Figure 3d with labels. Labels indicate IMG GeneID, annotated protein name, species, protein size. Nodes with boostrap values greater than or equal to 70% are indicated by black circles.

Supplementary table 1. Bacterial strains used in this study.

CE#	**ZG#**	**TND/ SAD#**	**Strain name in manuscript**	**Genotype**	**Figure ('S' denotes supplemental figure)**
CE1		SAD631	Wildtype (WT)	*Acinetobacter baylyi* ADP1	1A, S1B
CE100		SAD2537	Pil-cys or Parent	ADP1 *comP*^{T129C}	1A, 2A, 2C, 2D, 3A, 4B, 4D, S1B, S2B, S4B
CE329	ZG1709		Δ*pilT*	ADP1 Δ*pilT*::*spec*	1A
CE317		TND0779	Pil-cys Δ*pilT* or Parent	ADP1 *comP*^{T129C} Δ*pilT*::*spec*	1A, 1C, 2A, 2C, 3B, S4A
CE2	ZG1693		Δ*pilG*	ADP1 *comP*^{T129C} Δ*pilG*	S4B
CE3	ZG1694		Δ*pilH*	ADP1 *comP*^{T129C} Δ*pilH*	S4B
CE8	ZG1695		Δ*pilI*	ADP1 *comP*^{T129C} Δ*pilI*	S4B
CE9	ZG1696		Δ*pilJ*	ADP1 *comP*^{T129C} Δ*pilJ*	S4B
CE10	ZG1697		Δ*chpA*	ADP1 *comP*^{T129C} Δ*chpA*	S4B
CE122	ZG1698		Δ*ompA*	ADP1 *comP*^{T129C} Δ*ompA*::*kan*	S4B
CE233	ZG1699		Δ*fimL*	ADP1 *comP*^{T129C} Δ*fimL*::*kan*	S4B
		TND0114	Δ*comP*	ADP1 Δ*comP*::*kan*	3A, S4B
CE6	ZG1668		Δ*pilG* Δ*pilT*	ADP1 *comP*^{T129C} Δ*pilG* Δ*pilT*::*kan*	1C, 1D, S4A
CE7	ZG1669		Δ*pilH* Δ*pilT*	ADP1 *comP*^{T129C} Δ*pilH* Δ*pilT*::*kan*	1C, 1D, S4A
CE18	ZG1670		Δ*pilI* Δ*pilT*	ADP1 *comP*^{T129C} Δ*pilI* Δ*pilT*::*kan*	1C, 1D, S4A

CE19	ZG1671		Δ*pilJ* Δ*pilT*	ADP1 *comP*^{T129C} Δ*pilJ* Δ*pilT*::*kan*	1C, 1D, S4A
CE20	ZG1672		Δ*chpA* Δ*pilT*	ADP1 *comP*^{T129C} Δ*chpA* Δ*pilT*::*kan*	1C, 1D, S4A
CE312	ZG1675		Δ*ompA* Δ*pilT*	ADP1 *comP*^{T129C} Δ*ompA*::*kan* Δ*pilT*::*spec*	1C, 1D, S4A
CE315	ZG1676		Δ*fimL* Δ*pilT*	ADP1 *comP*^{T129C} Δ*fimL*::*kan* Δ*pilT*::*spec*	1C, 1D, S4A
CE256	ZG1681		PilQ-mCherry or Parent	ADP1 *comP*^{T129C} *pilQ*::*pilQ-mCherry, gent,* P_{tac}- *aroK*	S2B, S2C
CE331	ZG1682		PilQ-GmR	ADP1 *comP*^{T129C} *pilQ*::*pilQ, gent,* P_{tac}-*aroK*	S2B
CE320	ZG1700		Δ*pilG*	ADP1 *comP*^{T129C} *pilQ*::*pilQ-mCherry, gent,* P_{tac}- *aroK* Δ*pilG*	S2C
CE321	ZG1701		Δ*pilH*	ADP1 *comP*^{T129C} *pilQ*::*pilQ-mCherry, gent,* P_{tac}- *aroK* Δ*pilH*	S2C
CE322	ZG1702		Δ*pilI*	ADP1 *comP*^{T129C} *pilQ*::*pilQ-mCherry, gent,* P_{tac}- *aroK* Δ*pilI*	S2C
CE323	ZG1703		Δ*pilJ*	ADP1 *comP*^{T129C} *pilQ*::*pilQ-mCherry, gent,* P_{tac}- *aroK* Δ*pilJ*	S2C
CE324	ZG1704		Δ*chpA*	ADP1 *comP*^{T129C} *pilQ*::*pilQ-mCherry, gent,* P_{tac}- *aroK* Δ*chpA*	S2C
CE325	ZG1705		Δ*ompA*	ADP1 *comP*^{T129C} *pilQ*::*pilQ-mCherry, gent,* P_{tac}- *aroK* Δ*ompA*::*kan*	S2C

CE326	ZG1706		ΔACIAD0653	ADP1 *comP*^{T129C} *pilQ*::*pilQ-mCherry, gent,* P_{tac}- *aroK* Δ ACIAD0653::*kan*	S5
CE327	ZG1707		ΔACIAD0898	ADP1 *comP*^{T129C} *pilQ*::*pilQ-mCherry, gent,* P_{tac}- *aroK* Δ ACIAD0898::*kan*	S5
CE328	ZG1708		Δ*fimL*	ADP1 *comP*^{T129C} *pilQ*::*pilQ-mCherry, gent,* P_{tac}- *aroK* Δ*fimL*::*kan*	S2C
CE17	ZG1686		Parent	ADP1 *comP*^{T129C} *pilG*::*pilG-mRuby3*	1E, S3B
CE40	ZG1687		Δ*chpA*	ADP1 *comP*^{T129C} *pilG*::*pilG-mRuby3* Δ*chpA*	1E, S3B
CE127	ZG1688		Δ*ompA*	ADP1 *comP*^{T129C} *pilG*::*pilG-mRuby3* Δ*ompA*::*kan*	1E, S3B
CE257	ZG1689		Δ*fimL*	ADP1 *comP*^{T129C} *pilG*::*pilG-mRuby3* Δ*fimL*::*chlor*	1E, S3B
CE261	ZG1690		Δ*pilI*	ADP1 *comP*^{T129C} *pilG*::*pilG-mRuby3* Δ*pilI*	1E, S3B
CE341	ZG1691		Δ*pilH*	ADP1 *comP*^{T129C} *pilG*::*pilG-mRuby3* Δ*pilH*	1E, S3B
CE342	ZG1692		Δ*pilJ*	ADP1 *comP*^{T129C} *pilG*::*pilG-mRuby3* Δ*pilJ*	1E, S3B
CE25	ZG1736		PilG-mRuby3 Δ*pilT*	ADP1 *comP*^{T129C} *pilG*::*pilG-mRuby3* Δ*pilT*::*kan*	S3A
CE150	ZG1680		Δ*pilC*	ADP1 *comP*^{T129C} Δ*pilC*	2C, 2D
CE16	ZG1678		Δ*pilY1*	ADP1 *comP*^{T129C} Δ*pilY1*	2C, 2D

CE66	ZG1679		Δ*pilQ*	ADP1 *comP*^{T129C} Δ*pilQ*	2C, 2D, S1B, S2B
CE286		TND2544	Δ*comEA*	ADP1 *comP*^{T129C} Δ*comEA*::*kan*	2C, 2D
CE287		TND2546	Δ*comEC*	ADP1 *comP*^{T129C} Δ*comEC*::*kan*	2C, 2D
CE289		TND2556	Δ*comM*	ADP1 *comP*^{T129C} Δ*comM*::*kan*	2C, 2D
CE22	ZG1683		Δ*pilB*	ADP1 *comP*^{T129C} Δ*pilB*	3A, 3C, 4G
CE67	ZG1685		Δ*pilB2*	ADP1 *comP*^{T129C} Δ*pilB2*	3A, 3C, 4G
CE54	ZG1684		Δ*pilB* Δ*pilB2*	ADP1 *comP*^{T129C} Δ*pilB* Δ*pilB2*::*kan*	3A, 3C, 4G
CE310	ZG1673		Δ*pilB* Δ*pilT*	ADP1 *comP*^{T129C} Δ*pilB* Δ*pilT*::*spec*	3B, 3C, 4F
CE311	G1674		Δ*pilB2* Δ*pilT*	ADP1 *comP*^{T129C} Δ*pilB2* Δ*pilT*::*spec*	3B, 3C, 4F
CE316	ZG1677		Δ*pilB* Δ*pilB2* Δ*pilT*	ADP1 *comP*^{T129C} Δ*pilB* Δ*pilB2*::*kan* Δ*pilT*::*spec*	3B, 3C
CE263		TND1201	Δ*cpiR*	ADP1 *comP*^{T129C} Δ*cpiR*::*kan*	4B, 4E
CE264		SAD2792	Δ*cpiR* Δ*cpiA*	ADP1 *comP*^{T129C} Δ*cpiRA*::*kan*	4B, 4E
		TND2260	P_{tac}-*cpiA*	ADP1 *comP*^{T129C} igACIAD0096-ACIAD0098::*Cm*^{R}-P_{tac}-*cpiA*	4B
		TND2093	P_{cpiA}-GFP Parent	*V. cholerae* E7946 *Sm*^{R} Δ*lacZ*::*SpecR*-P_{cpiA}-*gfp*	4C
		TND2126	P_{cpiA}-GFP P_{BAD}-*cpiR*	*V. cholerae* E7946 *Sm*^{R} Δ*lacZ*::*SpecR*-P_{cpiA}-*gfp* ΔVCA0692::*Carb*^{R}-P_{BAD}-*cpiR*	4C
		TND1335	*cpiA*-FLAG	ADP1 *comP*^{T129C} *cpiA*-3X FLAG	4D
		TND1284	*cpiA*-FLAG Δ*cpiR*	ADP1 *comP*^{T129C} *cpiA*-3X FLAG Δ*cpiR*::*kan*	4D

CE282		SAD2808	Δ*pilB* Δ*cpiR*	ADP1 *comP*^{T129C} Δ*pilB* Δ*cpiR*::*kan*	4E, 4G
CE283		SAD2806	Δ*pilB2* Δ*cpiR*	ADP1 *comP*^{T129C} Δ*pilB2* Δ*cpiR*::*kan*	4E, 4G
CE284		SAD2809	Δ*pilB* Δ*cpiR* Δ*cpiA*	ADP1 *comP*^{T129C} Δ*pilB* Δ*cpiRA*::*kan*	4E
CE285		SAD2807	Δ*pilB2* Δ*cpiR* Δ*cpiA*	ADP1 *comP*^{T129C} Δ*pilB2* Δ*cpiRA*::*kan*	4E, 4G
CE265		SAD2645	Δ*cpiR* Δ*pilT*	ADP1 *comP*^{T129C} Δ*cpiR*::*kan* Δ*pilT*::*spec*	4E, 4F
CE266		SAD2810	Δ*cpiR* Δ*cpiA* Δ*pilT*	ADP1 *comP*^{T129C} Δ*cpiRA*::*kan* Δ*pilT*::*spec*	4E
CE302		SAD2822	Δ*pilB* Δ*cpiR* Δ*pilT*	ADP1 *comP*^{T129C} Δ*pilB* Δ*cpiR*::*kan* Δ*pilT*::*spec*	4E, 4F
CE303		SAD2820	Δ*pilB2* Δ*cpiR* Δ*pilT*	ADP1 *comP*^{T129C} Δ*pilB2* Δ*cpiR*::*kan* Δ*pilT*::*spec*	4E, 4F
CE304		SAD2823	Δ*pilB* Δ*cpiR* Δ*cpiA* Δ*pilT*	ADP1 *comP*^{T129C} Δ*pilB* Δ*cpiRA*::*kan* Δ*pilT*::*spec*	4E
CE305		SAD2821	Δ*pilB2* Δ*cpiR* Δ*cpiA* Δ*pilT*	ADP1 *comP*^{T129C} Δ*pilB2* Δ*cpiRA*::*kan* Δ*pilT*::*spec*	4E, 4F

CE strains available upon request from CKE, ZG strains available upon request from ZG, TND or SAD strains available upon request from ABD.

Supplementary table 2. Primers used for strain construction.

Primer name	**Primer sequence 5' → 3' (overlapping regions underlined, point mutations in bold)**	**Description**
DOG0175	AAACTATCCAGATAAGGGAAAGC	comP F1
CEdalia87	GAAGTTGTCGTACATTTCCA**ACA**TACAGCGCCACTAGCATATG	comPT129C R1
CEdalia88	CATATGCTAGTGGCGCTGTA**TGT**TGGAAATGTACGACAACTTC	comPT129C F2
DOG0178	AGGATCTGTAATGACGGGTTGAG	comP R2
DOG0176	GTCGACGGATCCCCGGAATCATAAAATTTCTCCACCAATGTTG	ΔcomP R1
DOG0177	GAAGCAGCTCCAGCCTACATGATAGTAGTACTATATGGCTTTAAAAG	ΔcomP F2
ABD123	ATTCCGGGGATCCGTCGAC	AbR cassette F
ABD124	TGTAGGCTGGAGCTGCTTC	AbR cassette R
BBC1934	GTTACAAAGTCAGGGACGTAAAG	ΔpilT F1
BBC1935	GTCGACGGATCCCCGGAATATCCATATTTTCCCCGAAGATCG	ΔpilT R1
BBC1936	GAAGCAGCTCCAGCCTACATAAGAATAACGCTACTCGATCTG	ΔpilT F2
BBC1939	GGTATTCAGATTGATCGTCAGTTAG	ΔpilT R2
CE31	GCTGTTTGATTTTATCCAGAACCTTG	ΔpilG F1
CE61	TGACGTGATTACGAATTGCGGTGATTTTGATCACTTTGGATTTGTCTTCC	ΔpilG R1
CE62	GGAAGACAAATCCAAAGTGATCAAAATCACCGCAATTCGTAATCACGTCA	ΔpilG F2
CE34	GCGCTGTAATTACAATAGTGTTCGGA	ΔpilG R2 and pilG-mRuby3 R2
CE37	GGTGGTACGCAGTTGTGGTAAAAT	ΔpilH F1 and pilG-mRuby3 F1

CE63	ATCATCCGTATGAATATATTGCTGGATTGAATCATCAACAATCAAAATACGTGCCA	ΔpilH R1
CE64	TGGCACGTATTTTGATTGTTGATGATTCAATCCAGCAATATATTCATACGGATGAT	ΔpilH F2
CE40	GGCAACTCAATTCAAACTGATGTACTT	ΔpilH R2
CE101	TTCAACGCTCATTCGTTGCCAT	ΔpilI F1
CE102	ATCAATATTGTGAAGCATTCATAAAATCTGTCAAACCAGCAGATGTGGTTGC	ΔpilI R1
CE103	GCAACCACATCTGCTGGTTTGACAGATTTTATGAATGCTTCACAATATTGAT	ΔpilI F2
CE104	CAGTTGACTGGTTACTGGTTCTGC	ΔpilI R2
CE107	GGTTTTTCCAGTTTTTAATGCTGCC	ΔpilJ F1
CE108	TCAGATGCAAAATCAAGCTTATACGTCGCTTTATTTTTTTTCCGATTGATTGA	ΔpilJ R1
CE109	TCAATCAATCGGAAAAAAAATAAAGCGACGTATAAGCTTGATTTTGCATCTGA	ΔpilJ F2
CE110	CCGAACAGTACGCTGCAATC	ΔpilJ R2
CE29	AATATCTTGTCGCCGATTCATTGAAA	ΔchpA F1
CE113	GGTTTTGGCTATGTTTAATCGCTTTCGTCTCTATAAGATGATTTACTTGTGCA	ΔchpA R1
CE114	TGCACAAGTAAATCATCTTATAGAGACGAAAGCGATTAAACATAGCCAAAACC	ΔchpA F2
CE115	CTGTATTTTGATGCAATGTTGGAGATT	ΔchpA R2
CE502	AATGGTGGGCCGTGAAAAAGC	ΔompA F1
CE503	GTCGACGGATCCCCGGAATAGTAGCAAGTGCAATACGACTCAATTTc	ΔompA R1
CE504	GAAGCAGCTCCAGCCTACAGTTCAACCTGGTCAACAAGCTCC	ΔompA F2

CE505	CCAGATCAGATACCAGATCAGGTGATTAT	ΔompA R2
CE735	GTGCACTGGGGATATCTGCACT	ΔfimL F1
CE736	GTCGACGGATCCCCGGAATATCGAAGCGAATAGAAACTTGTGAAGAC	ΔfimL R1
CE737	GAAGCAGCTCCAGCCTACAAACGCCTCCCAATTTCAATCAACG	ΔfimL F2
CE738	TGCTAACAGAATTGTATGTGTCTACGCC	ΔfimL R2
CE590	ATGAGAACAGATTTTAACGTTTTTACGACTGG	PilQ-mCherry up F
CE196	GAACCAGCAGCTGAACCAGCTGAACCATGATTTCCAACAATAGTGTCATTAACTATTCG	PilQ-mCherry up R
CE197	TTCAGCTGCTGGTTCAGGTGAATTTATGGTTTCCAAGGGCGAGGA	PilQ-mCherry mCherry region F
CE198	TTACTTGAATTAAAACTATATTATTTGTACAGCTCATCCATGCCA	PilQ-mCherry mCherry region R
CE637	TATAGTTTTAATTCAAGTAATTCAATAGGTGACTCCATTCCGGGGATCCGTCGAC	PilQ-mCherry AbR region F1
CE593	TCGTTGCTGCTGCGTAACATGCGAAACTATCCTCATCCTGTCTCTTG	PilQ-mCherry AbR region R1
CE594	CAGGATGAGGATAGTTTCGCATGTTACGCAGCAGCAACGATG	PilQ-mCherry AbR region F2
CE595	GGAACTTCAAGATCCCCTTATTAGGTGGCGGTACTTGGGTC	PilQ-mCherry GmR region R2
CE596	GACCCAAGTACCGCCACCTAATAAGGGGATCTTGAAGTTCCTATTCCG	PilQ-mCherry Ptac region F
CE336	GCTTAATTACCTCCTAATTGAATTCCTAGGC	PilQ-mCherry Ptac region R
CE638	GGAATTCAATTAGGAGGTAATTAAGCTTGCCAAGCAAAGAGTTTGACACC	PilQ-mCherry down F

CE592	TCTAATGCCGCTGCACTGTCAC	PilQ-mCherry down R
CE546	CCAGATCTCTACGCATTTCACCG	ΔACIAD0653 F1
CE547	GTCGACGGATCCCCGGAATGACCCCAAGAATAGATATTTTGATTGAGTTGT	ΔACIAD0653 R1
CE548	GAAGCAGCTCCAGCCTACACGCGTTGCAATTGTAATCGTTCC	ΔACIAD0653 F2
CE549	GTAGAAGGGTCTCATGTTGCGGG	ΔACIAD0653 R2
CE552	CACAATACGTCCCAGCAATTGAAAC	ΔACIAD0898 F1
CE553	GTCGACGGATCCCCGGAATGACTAGTGCACGCATTGCATGC	ΔACIAD0898 R1
CE554	GAAGCAGCTCCAGCCTACAGAGATTAGCATTTACGAACGTCAATAAGCG	ΔACIAD0898 F2
CE555	CGACACATGTTTGCTCTGCATCC	ΔACIAD0898 R2
CE146	TTCACCTGAACCAGCAGCTGAACCAGCTGAACCTACACTGACGTGATTACGAATTGCG	pilG-mRuby3 R1
CE147	TGGTTCAGCTGCTGGTTCAGGTGAATTTATGGTATCTAAGGGTGAAGAATTGATTAAGG	mRuby3 F
CE148	TTACTTATATAATTCATCCATTCCACCCCCAAG	mRuby3 R
CE149	GGGTGGAATGGATGAATTATATAAGTAACACGATATTGTTTTGAGGTCTTTATGGCAC	pilG-mRuby3 F2
CE389	TCAGGAAGTTGCCTGAACCTGA	ΔpilC F1
CE390	ACAGAGCCCATTTGGAAAATTGGTGGCATTACTTGCGTTTTTTTTGCT	ΔpilC R1
CE391	AGCAAAAAAAACGCAAGTAATGCCACCAATTTTCCAAATGGGCTCTGT	ΔpilC F2
CE392	TTGAAAAGCTGGCTGGCCTTC	ΔpilC R2
CE136	TTGGTCGATAATGCAGATCAGCT	ΔpilY1 F1
CE137	GGGGTGCTTTGCTCATACCATTTTAAGAGATACTGAGTGTATATCGATTTTTTCAT	ΔpilY1 R1

CE138	ATGAAAAAATCGATATACACTCAGTATCTCTTAAAATGGTATGAGCAAAGCACCCC	ΔpilY1 F2
CE139	GCAGGGATATCAGATTTTAACTGTGC	ΔpilY1 R2
CE85	AATAAGAGCGAATAGCAAACTAATTGTCG	ΔpilQ F1
CE340	TTTCCAACAATAGTGTCATTAACTATTCGAGTCGTAAAAACGTTAAAATCTGTTCTCAT	ΔpilQ R1
CE341	ATGAGAACAGATTTTAACGTTTTTACGACTCGAATAGTTAATGACACTATTGTTGGAAA	ΔpilQ F2
CE88	AGCGTATAACGATCAATTACTTCGC	ΔpilQ R2
BBC1891	AATCACTTGAAGTGCAGATTCG	ΔcomEA F1
BBC3451	GTCGACGGATCCCCGGAATATGACGTATTGACATGAATTAACC	ΔcomEA R1
BBC3452	GAAGCAGCTCCAGCCTACATAAGAGGCTGAGTCATGCTCAAAATAC	ΔcomEA F2
BBC1894	ATCTTCACCTTCTCCAAACTGG	ΔcomEA R2
DOG0180	AGTATTTGAGTTCGGGTATTATTGC	ΔcomEC F1
DOG0181	GTCGACGGATCCCCGGAATCATGGCAATGCCAGCAATC	ΔcomEC R1
DOG0182	GAAGCAGCTCCAGCCTACAAAGGGAGCGATTCATTTTAAGTTTG	ΔcomEC F2
DOG0183	TTACTCAAGCCGTTACAGTTCTG	ΔcomEC R2
DOG0140	GTTGCTGCATTTGTTCGATCTG	ΔcomM F1
DOG0141	GTCGACGGATCCCCGGAATCATACTATTATTGTTCCATTATGGTGC	ΔcomM R1
DOG0142	GAAGCAGCTCCAGCCTACATATCGCAGTGAACATAGCTAAAA	ΔcomM F2
DOG0143	ATCAGTGGTTGGGAAGGTG	ΔcomM R2
CE23	TTATGACTATCAATCTCAAGCACATGCT	ΔpilB F1
CE93	ATTCACTGGTTACACGATTAATTTCCTGAAACTTAGGTGGTGTTGTAAATGCTG	ΔpilB R1
CE94	CAGCATTTACAACACCACCTAAGTTTCAGGAAATTAATCGTGTAACCAGTGAAT	ΔpilB F2

CE26	CTTTCATGGCGTGTTTGTCGTG	ΔpilB R2
CE210	AAGCCAACCATAATCCGATTGTGAC	ΔpilB2 F1
CE328	TGGGACCACCCTTAAGACTTCTTCCCATTGTGTATCTATTTCAAAATGATATGTCAT	ΔpilB2 R1 (in frame)
CE329	ATGACATATCATTTTGAAATAGATACACAATGGGAAGAAGTCTTAAGGGTGGTCCCA	ΔpilB2 F2 (in frame)
CE213	CTCACGCCACCCAATCAAGAC	ΔpilB2 R2
CE240	GTCGACGGATCCCCGGAATTTATTTCTCCCCCACACCATTCAC	ΔpilB2 R1 (AbR disruption)
CE241	GAAGCAGCTCCAGCCTACATAAAAGGTTAGTTTAGATCTTAAGATTCACCTCAT	ΔpilB2 F2 (AbR disruption)
DOG0130	CCTCTCCACTCGTTTCTAAAGAAC	ΔcpiR or ΔcpiA or cpiA-3X FLAG F1
DOG0131	GTCGACGGATCCCCGGAATCATAAGCCGATACTATCTGGATGG	ΔcpiR R1
DOG0132	GAAGCAGCTCCAGCCTACAGAAGTTCAATGTCAGTTAAAACATC	ΔcpiR F2
DOG0133	GACGTTGATTACGTAAATTTAATTCG	ΔcpiR or ΔcpiA or cpiA-3X FLAG R2
BBC921	GTCGACGGATCCCCGGAATTTGATCACTTACTAATTTCATTATCATTTAAATG	ΔcpiA R1
BBC922	GAAGCAGCTCCAGCCTACATAAAAAAGGACTGATTTCTCAGCCC	ΔcpiA F2
BBC2565	TCCACCACTTCCACCTGCATTTTCATGAAACACTTGCTGC	cpiA-3X FLAG R1
BBC2570	GCAGGTGGAGCAGGTGGATAAAAAAGGACTGATTTCTCAGCCC	cpiA-3X FLAG F2
BBC2272	GCAGGTGGAAGTGGTGGAGATTATAAAGACCATGATGGTGACTACAAGGATCACGACATTGATTATAAGGATGACGATGACAAAGCAGGTGGAGCAGGTGGA	3X FLAG MIDDLE F

BBC2273	TCCACCTGCTCCACCTGCTTTGTCATCGTCATCCTTATAATCAATGTCGTGATCCTTGTAGTCACCATCATGGTCTTTATAATCTCCACCACTTCCACCTGC	3X FLAG MIDDLE R
DOG0229	CAATTTCACACAGGATCCCGGGAGGAGGTAACGTAATGATAATGAAATTAGTAAGTGATCAAATTC	Amplify *cpiA* for P_{tac}-*cpiA* construct F
DOG0230	TGTAGGCTGGAGCTGCTTCTTAATTTTCATGAAACACTTGCTGC	Amplify *cpiA* for P_{tac}-*cpiA* construct R
BBC3072	CACCATTATGATGGCAATCGTATGATTCGAAGTATGTGAAAAATCTGC	Amplify P_{cpiA} for P_{cpiA}-GFP F
BBC3074	CCCGGGATCCTGTGTGAAATTGACTAGCAGTATTGTATTACAAAACTTTTG	Amplify P_{cpiA} for P_{cpiA}-GFP R
BBC3075	CAATTTCACACAGGATCCCGGGAGGAGGTCGGCTTATGGATATAGGTCGC	Amplify *cpiR* for P_{BAD}-*cpiR* construct F
BBC2560	TGTAGGCTGGAGCTGCTTCTTACTTTTTAGTGTCTATCAAAGTAAAAATGAGATG	Amplify *cpiR* for P_{BAD}-*cpiR* construct R